On the Mechanisms of OH Radical Induced DNA-Base Damage: A Comparative Quantum Chemical and Car−Parrinello Molecular Dynamics Study†

Yudong Wu,‡ Christopher J. Mundy,*,§ Michael E. Colvin,|| and Roberto Car‡

Department of Chemistry and Princeton Materials Institute, Princeton University, Princeton, New Jersey 08544, Computational Chemical Biology, Chemistry and Materials Science L-091 Lawrence Livermore National Laboratory, Livermore, California 94550, and Schools of Natural Science and Engineering, University of California, Merced, Calfornia 95344

Received: August 8, 2003; In Final Form: November 25, 2003

Understanding the basic chemistry of the interaction of radicals with DNA bases is imperative when trying to predict the potential effects of radiation on DNA. Experimental evidence points to guanine as having the highest affinity of all the DNA bases for undergoing damage. However, radiation-induced damage to other bases may also have important health effects, and therefore the reactions of other DNA bases are also of interest. To this end, numerous studies have been performed on thymine to elucidate its role in the initial phases of DNA damage. To date, the theoretical studies on this topic have only dealt with reaction energetics in the gas phase or within a continuum solvent model. We present a detailed Car−Parrinello molecular dynamics study of DNA bases in explicit water interacting with an OH radical. Our findings indicate that the specific mechanisms of the initial phase of DNA damage are different in thymine and guanine, which is consistent with experiment-based conjectures on this subject. We also compare the effects of different exchange and correlation functionals on the proposed reaction energetics as well as a comparison with traditional quantum chemistry methods. Our deduced mechanisms are consistent with the experimentally observed products.

Introduction

Understanding the basic chemistry of the initial stages of DNA-base damage has far-reaching implications for radiation therapy, health effects of radiation exposure, and aging.[1] Although there are numerous experimental studies on the initial phases of DNA-base oxidation, there are still open questions as to the precise mechanisms.[2−11] One set of experiments elucidates the nature of DNA-base damage through direct chemical reaction of the native bases with various oxidizing agents.[5−7,12] The result of the oxidizing process seems to be highly dependent on the oxidizing reagent and the conditions under which the reaction takes place. Previous theoretical studies on this subject have been mostly concerned with computing the relative stability of various radicals as well as electron affinities and ionization potentials for a variety of DNA bases.[13−18] Calculations have also gone beyond the single base to include the effects of hydrogen bonding and stacking on radical stabilization as well as mechanisms for base repair.[13,19] All of the previously mentioned calculations have used static quantum chemical methods based in density-functional theory (DFT) and atom-centered Gaussian basis sets. The advantage of calculations using such basis sets, vs the plane-wave methods used in the dynamical calculations described below, is the ease of including exact exchange terms in the functional, as in the Becke-3-Lee−Yang−Parr (B3LYP) hybrid functional.[20]

We recently published a theoretical study focused on using dynamical methods to try to elucidate possible reaction mechanisms for the initial stages of oxidation in guanine.[21] In this study, both traditional static quantum chemical methods and the Car−Parrinello molecular dynamics (CPMD) method were used to investigate and identify transition states and reaction mechanisms for an isolated guanine interacting with an OH radical. The salient feature of this study is that many of the proposed mechanisms of the initial stages of guanine oxidation were identified.[10] By use of Wannier centroid (WC) analysis to track the electronic degrees of freedom, we were able to provide a picture that indicated that a two-step mechanism for oxidation of guanine was possible, namely, electron transfer followed by proton extraction. This finding was independently corroborated by using natural population analysis (NPA) to determine the degree of charge transfer.[21] Both the WC and NPA analyses were in very good agreement, indicating that well-converged plane-wave pseudopotential calculations agree well with traditional static all-electron quantum chemical methods. Although the gas-phase CPMD and static calculations were able to give new insights in both the dual use of simulation methodology and the possible mechanisms leading to DNA-base damage, there are still improvements needed in order to make closer contact with experimental observations.

One such choice is the inclusion of solvent effects on the observed dynamics. There are two ways to incorporate solvent effects into quantum chemical calculations. The use of a continuum solvent in conjunction with static methods has become an acceptable way to treat the effects of the solvent. In this approximation, the molecule interacts with an electrostatic potential derived from a continuous surrounding media with a particular dielectric constant. The resulting approach has been shown in many cases to yield quantitative solvation energies and will at minimum give the correct qualitative description of the stabilization of intermediates due to the particular environ-

† Part of the special issue "Fritz Schaefer Festschrift".

* Author to whom correspondence may be addressed. E-mail: mundy2@llnl.gov.

‡ Princeton University.

§ Lawrence Livermore National Laboratory.

|| University of California.

10.1021/jp0363592 CCC: $27.50
Published on Web 02/25/2004

ment. Although such continuum models extend the utility of "static" quantum chemical methods, they cannot wholly replace dynamical explicit solvent models. First, there are many cases, especially for reacting systems, where the explicit waters directly participate in the reactions. Second, molecular dynamics can provide phase-space sampling at finite temperature. Moreover, dynamical simulations including explicit solvent molecules can provide a more complete picture of the complex kinetics of the solution phase reaction path. For example, when using static methods to calculate the aqueous phase reaction energies, the reactants are typically taken to be the *isolated* reactant molecules since these are easily characterized stationary points on the potential-energy surface. In the dynamical simulations, the actual reaction may occur from a transient reaction complex that is considerably lower in energy than the separated molecules. It is clear that examining the effects of *explicit* solvent on the dynamics and energetics of DNA-base oxidation would be a useful contribution from two points of view. First, such calculations would more accurately mimic the experimental studies. Second, such explicit solvent simulations provide a means of evaluating the much less computationally intensive continuum solvent models. Our results, in conjunction with other theoretical studies on DNA-base radicals will give a more complete picture to experimentalists when trying to interpret their complex data.[13−18]

In this study, we perform calculations on thymine and guanine in the presence of explicit water to further elucidate the initial stages of DNA-base damage. We choose guanine because of its high affinity of undergoing oxidation as well as to build on our previous gas-phase simulations.[21] We choose thymine because it has also been implicated in radiation-induced DNA damage, and as a pyrimidine base, it will provide an interesting contrast to the purinic guanine. Both of these DNA bases are also well characterized experimentally and have been studied extensively undergoing oxidation.[5,11] It has been conjectured from experimental observations that the initial stages of oxidation are different for guanine and thymine, and the precise nature of the oxidative process is still in question.[5,11] As is now the precedent, we will make use of both static and dynamical methods to compare different aspects of theory (dependence on basis set and exchange and correlation functional), resulting in a more complete picture of possible mechanisms of an irradiated DNA base.

Computational Details

We used two different implementations to perform CPMD.[22] We used the CPMD package[23] for the calculation on guanine and the CP90 package[24,25] for the calculations on thymine.

CPMD was implemented in a plane-wave basis within local-spin-density (LSD) functional theory.[22,23] The reactions of guanine with an OH radical in the presence of explicit waters were all performed with norm-conserving pseudopotentials for oxygen, hydrogen, nitrogen, and carbon,[26,27] with an energy cutoff of 70 Rydbergs (Ry) and with a Becke exchange and Lee−Yang−Parr (BLYP) gradient-corrected functional.[28,29] We used two different water box sizes in our guanine simulations. Initial configurations for the two solvated guanine systems were generated as follows. First, in a well-equilibrated cubic box of 32 waters with length 9.89 Å, all waters were removed within a distance of 1.5 Å of each guanine atom. This resulted in a configuration containing 21 water molecules. For the second source, we inserted a guanine molecule into a well-equilibrated box containing 64 waters in a box of triclinic symmetry with cell parameters (in Å) $a = (7.82, 7.82, 7.82)$, $b = (-7.82, 7.82, 7.82)$, and $c = (-7.82, -7.82, 7.82)$. Again, we removed water molecules within 1.5 Å from any guanine atom. This resulted in a configuration with 56 waters. Triclinic symmetry is chosen to more accurately represent spherical solvation. The reactions with OH were then initiated by removing a hydrogen from a selected water molecule to form the OH radical. WCs were calculated every 0.6 fs for the case of 21 solvating waters using the algorithm of Berghold et al.[30]

The reactions of thymine with OH are studied with the CP90 package. DFT within a plane-wave pseudopotential framework is used to calculate the interatomic forces. Perdew−Burke−Ernzerhof (PBE)-type[31]generalized gradient approximation (GGA) is adopted for the exchange and correlation energy. For the reactions in the gas phase, systems are simulated in a periodic repeating simple cubic unit cell with the length of 11.64 Å. The cell is large enough to avoid spurious interaction between periodic replica. Troullier−Martins-type norm-conserving pseudopotentials for C and H atoms are used.[32] Vanderbilt ultrasoft pseudopotentials[33] are used for oxygen and nitrogen. Energy cutoffs of 45 Ry for the wave functions and 200 Ry for the electron density are chosen. Second-order damped dynamics and preconditioning[34] are adopted to deal efficiently with geometry optimization and dynamics, leading to reaction products. To further speed up the calculation, the reactions of thymine with an OH radical in water were performed with Vanderbilt ultrasoft pseudopotentials for all atoms including hydrogen, carbon, oxygen, and nitrogen. Energy cutoffs of 25 Ry for the wave function and 200 Ry for the electron density are chosen. Simulation of a thymine in water is done similar to the approach taken for guanine described above. Water molecules (25) are present as a solvent in the simulation cell. Wannier functions are calculated every 0.36 fs using the scheme of Wu.[35]

We also perform nondynamical quantum chemical calculations to characterize individual points on the potential-energy surfaces for the reactions of thymine with OH. These quantum chemical calculations were performed using DFT with the B3LYP functional.[20] The molecular geometries were optimized with a 6-31G** basis, and the molecular entropies and thermal corrections to the free energies were calculated from the harmonic vibrational constants determined by analytic energy second derivatives calculated at the optimized B3LYP/6-31G** geometries. To estimate the effect of aqueous solvation on the relative energies, single-point energies were calculated at the B3LYP-optimized geometries using a dielectric continuum solvation model (COSMO)[36] coupled to the B3LYP/6-31G** wave functions. To compare the effects of different exchange-correlation functionals, the geometries of the thymine reaction products were reoptimized using the Becke and Lee−Yang−Parr (BLYP), Perdew-Wang 91 (PW91), and PBE functionals with a 6-31G** basis set. Unrestricted and restricted second-order Moller−Plesset perturbation-theory calculations were performed with an aug-cc-pVTZ basis set at the B3LYP/6-31G**-optimized geometries. All quantum chemical calculations were performed using Gaussian 98.[37]

Results and Discussion

Quantum Chemical Studies of Thymine. We have used quantum chemical predictions to study a series of dehydrogenation and hydroxylation products resulting from the reaction of thymine and a hydroxyl radical. These results are given in Tables 1 and 2 and Figures 1 and 2. For the dehydrogenation reactions of thymine (Figure 1), we find that the most easily abstracted hydrogen is on the C5 methyl group, with a highly

TABLE 1: Relative Energies of Dehydrogenated Thymine Radicals in Units of kJ/mol Calculated Using Different Exchange-Correlation Functionals[a]

	DFT					
dehydrogenation site	MP2/aug-cc-pVTZ	B3LYP (AE)	BLYP (AE)	PW91 (AE)	PBE (AE)	PBE (PP)
C5 methyl group	0.00	0.00	0.00	0.00	0.00	0.00
N3	161.28	131.13	102.45	106.87	105.80	109.35
C6	100.98	101.01	96.11	94.12	93.40	94.70
N1	40.44	28.88	23.13	29.37	28.86	36.92

[a] All electron (AE) calculations are done using the 6-31G** basis set except for MP2 calculations as noted and the Gaussian 98 package. Pseudopotential (PP) calculations are done using the CP90 package and plane-wave basis sets with energy cutoff of 45 Ry for the wave function and 200 Ry for the electron density. The numbering scheme of thymine is taken from Figure 3. All energies are relative to that of the most stable dehydrogenated thymine.

TABLE 2: Relative Energies of Hydroxylated Thymine Radicals in Units of kJ/mol Calculated Using Different Exchange-Correlation Functionals[a]

	DFT					
hydroxylation site	MP2/aug-cc-pVTZ	B3LYP (AE)	BLYP (AE)	PW91 (AE)	PBE (AE)	PBE (PP)
C5	9.36	16.10	16.34	12.89	12.98	17.51
C6	0.00	0.00	0.00	0.00	0.00	0.00
C4	148.48	100.82	88.06	88.16	88.25	89.77
C2	187.64	122.80	100.25	104.26	104.22	108.51

[a] Geometries are always reoptimized with exchange-correlation functionals. All electron (AE) calculations are done using the 6-31G** basis set except for MP2 as denoted and the Gaussian 98 package. Pseudopotential (PP) calculations are done using the CP90 package and plane-wave basis sets with an energy cutoff of 45 Ry for the wave function and 200 Ry for the electron density. The numbering scheme of thymine is taken from Figure 3. All energies are relative to that of the most stable hydroxylated thymine.

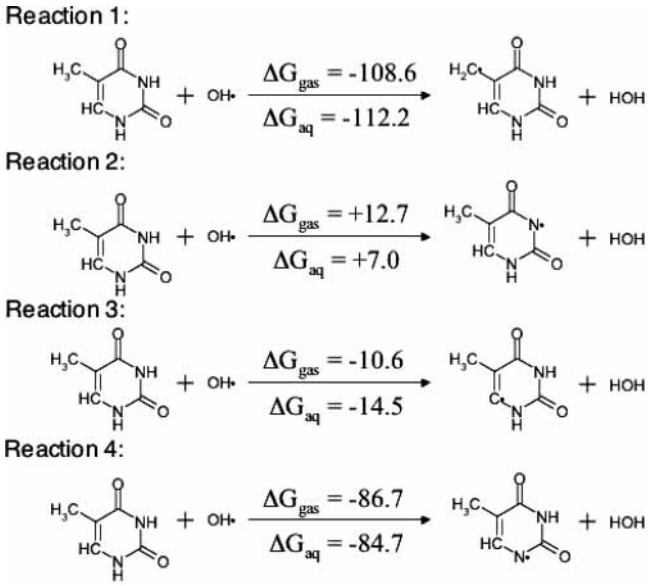

Figure 1. Gas- and aqueous-phase reaction energies of thymine and hydroxide radicals in kJ/mol. Energies are calculated at the B3LPY/6-31G**//B3LYP/6-31G** level of theory; solvation effects included use the COSMO solvation model.

favored gas-phase reaction free energy of −108.6 kJ/mol. This is followed by the N1 site at −86.7 kJ/mol. (Note that the N1 site in DNA is bound to the deoxyribose sugar and therefore does not contain a hydrogen to be abstracted.) The other potential dehydrogenation sites, N3 and C6, are considerably less thermodynamically favored. Inclusion of aqueous solvation

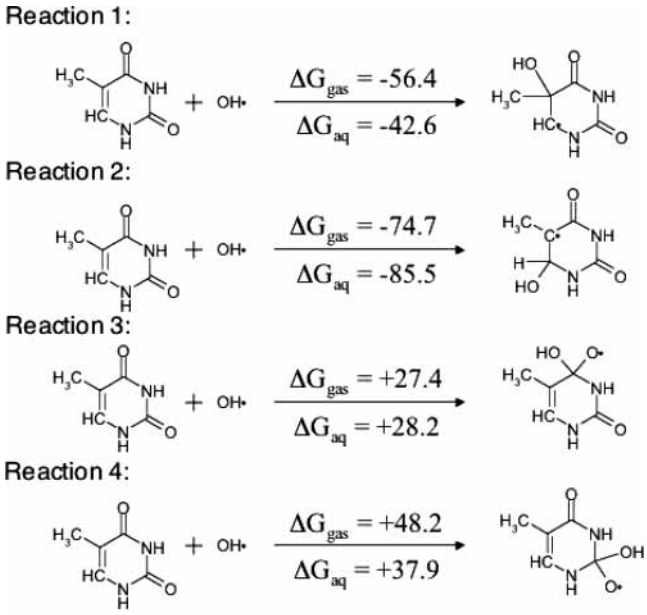

Figure 2. Gas- and aqueous-phase hydroxylation energies of thymine and hydroxide radicals in kJ/mol. Energies are calculated at the B3LYP/6-31G**//B3LYP/6-31G** level of theory; solvation effects included use the COSMO solvation model.

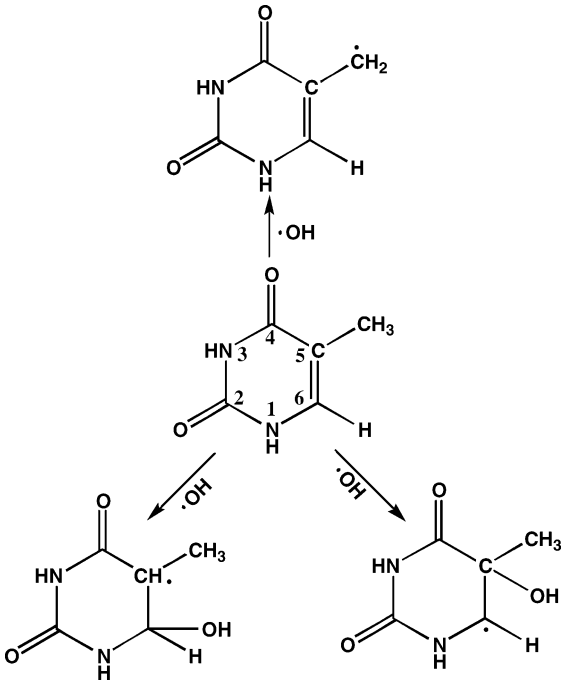

Figure 3. Experimentally proposed intermediates for the initial stages of thymine reacting with an OH radical.[5]

effects via a polarizable continuum model did not significantly affect the predicted dehydrogenation energies.

For the hydroxylation reactions (Figure 2), we find that OH attack at the C6 position is the most thermodynamically favored with a reaction free energy of −74.7 kJ/mol. The next most-favored site is the C5 at −56.4 kJ/mol. The two other possible hydroxylation sites, C2 and C4, were predicted to be thermodynamically unfavored, with reaction free energies of +48.2 and +27.4 kJ/mol, respectively. As with the dehydrogenation reactions, inclusion of aqueous solvation effects had minimal effect on the reaction energetics.

Figure 3 shows the reaction intermediates that have been experimentally isolated from the reactions of thymine with the

TABLE 3: Reaction Energies to Form Dehydrogenated Thymine Radicals in Units of kJ/mol Calculated Using Different Methods[a]

dehydrogenation (Figure 1)	ΔH_{MP2}	ΔH_{B3LYP}	ΔH_{BLYP}	ΔH_{PBE}	ΔG_{B3LYP}
reaction 1	−128.85	−106.44	−117.21	−121.46	−108.59
reaction 2	27.35	19.61	−19.83	−20.74	12.65
reaction 3	−26.68	−4.25	−19.92	−26.88	−10.58
reaction 4	−90.14	−79.29	−95.81	−94.33	−86.68

[a] All calculations are performed with Gaussian 98 using the 6-31G** basis sets except for the MP2 calculations performed using the aug-cc-pVTZ basis. The corrections for enthalpy and free energy were calculated from harmonic vibrational frequencies calculated with B3LYP/6-31G** at its optimized geometries.

TABLE 4: Reaction Energies to Form Hydroxylated Thymine Radicals in Units of kJ/mol Calculated Using Different Methods[a]

hydroxylation (Figure 2)	ΔH_{MP2}	ΔH_{B3LYP}	ΔH_{BLYP}	ΔH_{PBE}	ΔG_{B3LYP}
reaction 1	−113.70	−99.87	−99.96	−129.26	−56.41
reaction 2	−121.14	−114.04	−114.38	−140.31	−74.69
reaction 3	24.73	−15.83	−28.93	−54.67	27.39
reaction 4	62.25	4.51	−18.37	−40.33	46.18

[a] All calculations are done using Gaussian 98 with the 6-31G** basis sets except for the MP2 calculations performed using the aug-cc-pVTZ basis set. The corrections for enthalpy and free energy were calculated from harmonic vibrational frequencies calculated with B3LYP/6-31G** at its optimized geometries.

OH radical. It is through these intermediates shown in Figure 3 that result in observed damaged DNA products. In agreement with our predictions in Figure 1, the dehydrogenation is seen only to occur at the C5 site in thymine (as mentioned above the hydrogen at the N1 site is substituted by the deoxyribose sugar in DNA and is not available for abstraction). Also in agreement with our predictions in Figure 2, only hydroxylation products at the C5 and C6 sites of thymine are experimentally observed.

The effect of different DFT exchange-correlation functionals is shown in Tables 3 and 4 that list the reaction energies of the four dehydrogenation and hydroxylation reactions, respectively. Interestingly, the reaction energies of the thymine radicals vary appreciably depending on the choice of exchange and correlation functional, with a maximum variation for the dehydrogenation products of 29 kJ/mol between the B3LYP/6-31G** and BLYP/6-31G** results for the thymine N3 dehydrogenation and a maximum variation for the hydroxylation of 23 kJ/mol between the same two functionals for the thymine C2 hydroxylation site. The magnitude of this variation is large enough that the N3 dehydrogenation and C2 hydroxylation are predicted to be endothermic with the hybrid functional B3LYP and exothermic with other GGA-type functionals (BLYP, PW91, and PBE). (Note that both of these reaction products are much less thermodynamically favored than the other products, so this variation does not influence the predicted reaction products. See Tables 3 and 4.) It is not a priori obvious which of these functionals should yield the most accurate energetics; although since the B3LYP is a hybrid functional including exact electron exchange, it is likely that this would be the most reliable for organic radical systems. We investigated the possible role of spin contamination in these observed differences and found this to be a minimal effect. All S^2 values for these doublet states were less than 0.78. Across all compounds studied, the B3LYP functional systematically yielded S^2 values slightly (∼0.01) higher than from the BLYP, PW91, or PBE functionals. Large basis-set (aug-cc-pVTZ) unrestricted MP2 calculations at the B3LYP/6-31G**-optimized geometries for these compounds exhibited a high degree of spin contamination (S^2 values of 0.77 to 1.03) and yielded relative energies in poor agreement with the DFT results (data not shown). Restricted open-shell MP2/aug-cc-pVTZ energies at the B3LYP/6-31G** geometries are shown in Tables 1−4. The restricted MP2 energetics are in better agreement with the B3LYP/6-31G** energies, particularly for the most-favored reaction products, although MP2−B3LYP differences of up to 65 kJ/mol exist for the high-energy products.

Another variable in the calculations described in this paper is the inclusion of all electrons in the wave function vs replacing the core electrons with pseudopotentials. To make the CPMD simulations computationally feasible, pseudopotentials are used together with the plane-wave basis sets. Therefore, key questions are whether the core electrons contribute significantly to the chemical binding and whether the 45 and 200 Rydberg cutoffs used for the wave function and electron density are adequate. The pseudopotential results using the PBE functional are shown in Tables 1 and 2 to provide comparison with all-electron calculations and the localized Gaussian basis sets. By comparison of results derived with the PBE exchange and correlation functional, the maximum difference is 8 kJ/mol for the relative energy of the N1 vs C5 dehydrogenation products. This variation is small enough that the CPMD dynamics should yield reaction products consistent with the all-electron predictions.

Gas-Phase CPMD Thymine Simulations. *Dehydrogenation.* As was done in our previous study on guanine, we simulated the dehydrogenation reactions by starting with the OH radical 2.01 Å from the hydrogen to be abstracted (the C5 methyl site in the case of thymine), performing an initial wave-function optimization followed by molecular dynamics. These dynamics simulations yielded results similar to our recent study of guanine in that we find the dehydrogenation to be thermodynamically favored and to have no significant reaction barrier. However, the results for thymine differ from guanine in the mechanism of the dehydrogenation. Guanine, which is known to have the highest affinity of the DNA bases to undergo oxidation, was predicted to be spontaneously dehydrogenated by the OH radical at all sites via one of two possible mechanisms in the gas phase. In our recent study, we found that hydrogen abstraction could occur either by concerted electron−proton loss or electron transfer followed by proton loss.[21] In both mechanisms, we find that with hydrogen abstraction the electron is always removed from the π orbitals associated with the conjugated ring system and that no σ electron density is lost. This "proton-coupled" electron-transfer mechanism has been postulated both experimentally and theoretically.[10,38]

Our findings are different for dehydrogenation of thymine at the C5 methyl site. In the case of thymine, there seems to be no propensity for electron transfer to occur before proton transfer as is shown in the WC analysis in Figure 4. As is shown in Figure 5, the mechanism predicted by DFT for hydrogen abstraction occurs via σ electron loss at the C5 methyl site, yielding a product with the pyrimidine ring that retains a planar geometry. Furthermore, as was the case with guanine, we find hydrogen abstraction free energetically more favorable than hydroxylation (see Tables 3 and 4 and Figure 2). This is in contrast with experimental findings that indicate that most products formed involve OH addition.[5,7,12]

Hydroxylation. As shown in Figure 2, the quantum chemical simulations predict that hydroxylation is thermodynamically favored at the thymine C5 and C6 sites. In our dynamical simulations using pseudopotentials and the PBE functional, we find that the hydroxylation reactions at the C5 and C6 sites are

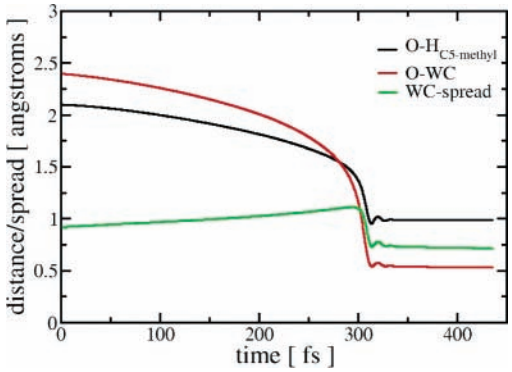

Figure 4. The evolution of the distances from the oxygen atom in the OH radical to the $H_{C5-methyl}$ in thymine and the WC of the electron moving with $H_{C5-methyl}$ during the dehydrogenation from the C5 methyl group in the gas phase. The hydrogen atom and the electron are moving concurrently. The spread of the WC is also shown; the σ electron becomes slightly delocalized when the oxygen atom approaches the $H_{C5-methyl}$ and fully localized between oxygen and hydrogen atoms as the O−H bond forms.

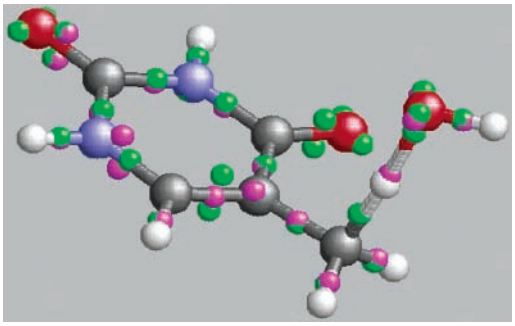

Figure 5. An intermediate state between reactants and products for hydrogen abstraction from the C5 methyl group of thymine in the gas phase. White, light black, cyan, red, magenta, and green balls correspond to hydrogen, carbon, nitrogen, and oxygen atoms and spin-up and spin-down electrons.

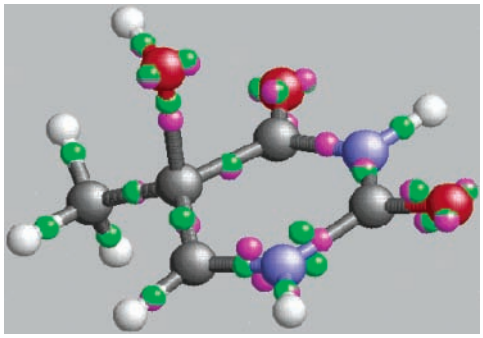

Figure 6. An intermediate state between reactants and products for the OH addition onto thymine at C5 in the gas phase. White, light black, cyan, red, magenta, green balls correspond to hydrogen, carbon, nitrogen, and oxygen atoms and spin-up and spin-down electrons.

thermodynamically favored and occur with no appreciable barrier. We initiate CPMD dynamics for OH addition by placing the OH radical 2.12 Å from the target sites. An initial wavefunction optimization is performed followed by molecular dynamics. Figure 6 shows an intermediate state between reactants and products for OH addition to the C5 site. The mechanism here shows π density being donated to form the new σ bond between C5 and the OH, leaving the pyrimidine ring in a distorted geometry.

Dynamical Simulations in Explicit Solvent. It is important to consider solvation effects for aqueous phase reactions involving radicals since ionic intermediates may be formed. Interactions with polar solvents stabilize reactive intermediates that would not appear if the reaction were to take place in a vacuum. A computationally efficient scheme to incorporate solvent effects is through the use of a COSMO as was done in the static quantum chemical calculations in Figures 1 and 2. In this section of the paper, the results for guanine are revisited in order to make a comparison to our previous gas-phase predictions[21] as well as a more direct comparison to thymine.

TABLE 5: Assigned Power Spectrum Frequencies of Guanine Both in the Gas and Solvated Conditions[a]

assigned stretch (Figure 7)	frequencies (cm^{-1}) gas phase	solvated (21 waters)	solvated (56 waters)
N2−H	3400	3360	3338
N1−H	3400	3126	3200
N9−H	3400	3130	3126
C8−H	3050	3100	3100

[a] All calculations were performed at 300 K for a duration of 1.5 ps. We choose to resolve the frequencies that are a result of N−H and C−H stretches that occur at high enough frequencies that require less statistics to resolve accurately. Since these frequencies will be the most affected by hydrogen bonding from solvating waters, we feel that they are representative for drawing conclusions regarding solvation.

Guanine. To determine the sensitivity of these results to reaction conditions, we investigate the same set of chemical reactions under solvated conditions, i.e., in the presence of explicit water. Explicit waters play two roles. The first is to solvate the guanine via hydrogen bonding and electrostatic interactions. The other is to provide solvation for the radical, increasing the propensity for complete charge transfer as was predicted from continuum solvent calculations.[21] To validate our model, we must demonstrate that we are including enough water to adequately reproduce solvated conditions. One way of achieving this is to compare a radial distribution function of oxygen and various guanine sites for the case of 21 and 56 solvating waters. Because we cannot average over many instances of the guanine, the simulation time required to produce a statistically smooth radial distribution function is prohibitive. Thus, we choose to compute the power spectrum of guanine in the gas phase and in the presence of 21 and 56 waters. The power spectrum (the Fourier transform of the velocity−velocity autocorrelation function) can be directly related to the infrared spectrum that is known to be extremely sensitive to solvation effects. Table 5 shows the frequencies as obtained from the power spectrum of 1.5-ps trajectories of the gas phase and solvated guanine. Note the extremely good convergence of the frequencies from 21 and 56 water simulations. Good agreement is found with experiments on alkylated guanine derivatives in an argon matrix.[39] Moreover, a recent comprehensive theoretical study of the infrared spectra of solvated uracil was performed using the same suite of computational methods outlined in the present study[40] and verified the existence of two solvation shells using 49 waters. Although it is difficult to make direct comparisons with this study, the good agreement between our redshifted frequencies for 21 and 56 waters as clearly shown in Table 5 indicates that the majority of the first solvation shell of guanine is adequately represented with 21 waters. Thus we proceed with the more computationally tractable 21 waters in our simulation of solvated guanine.

In our previously published study, although the OH addition was thermodynamically favored, the reaction was observed to occur in the gas phase from only a few selected starting

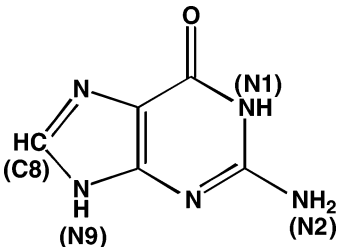

Figure 7. Schematic of the molecular structure of guanine with labels referring to reaction sites.

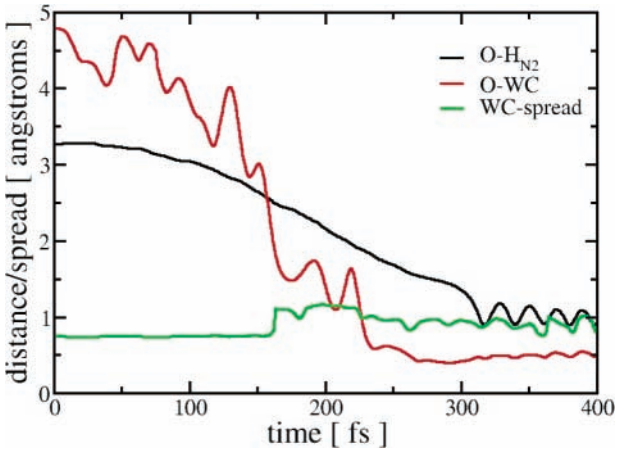

Figure 8. The evolution of the distances from the oxygen atom in the OH radical to the H_{N2} in guanine and the WC of the electron moving with H_{N2} during the hydrogen abstraction from the N2 in the gas phase. Electron transfer is complete before the proton transfers. The spread of the WC is also shown.

conditions. This leads to a key question of whether aqueous solvation will broaden the reaction channel for the OH addition. Another question arising for guanine−hydroxyl radical reactions in the gas phase is whether a different medium would allow an ionic mechanism, since we previously found that only partial electron transfer could occur due to the lack of any polar medium to stabilize an hydroxyl anion.[21] Finally, we would also like to investigate if any of the mechanistic results for guanine hold for the other DNA bases. In a previous study on dehydrogenation reactions of guanine with an OH radical, we compared the charge transfer indicated by the WCs obtained within CPMD to that of the NPA charge analysis that is obtained from traditional static quantum chemistry calculations.[21] This comparison confirms that there was a degree of charge transfer occurring before OH addition. We would like to better quantify this degree of charge transfer in the present study from examining the spread of the WC along the reacting trajectory. From previous studies on water, the spreads of the WC have been determined to be around 0.7 Å.[30,41]

We first re-examine the reacting trajectory that gave rise to dehydrogenation of the N2 (see Figure 7) hydrogen in the gas phase. Figure 8 shows the WC−O distance and the WC spread along the N2 reacting trajectory and indicates that there is no discernible collapse of the WC spread along the reacting trajectory. This is also corroborated from the previous NPA analysis that along the reacting CPMD trajectory there was a partial transfer of approximately −0.6 e onto the oxygen center.[21] The same dehydrogenation reaction in the presence of explicit waters tells a slightly different story (see Figure 9). Here it is apparent from the WC−O distance and the WC spread along the reacting trajectory that there is a large localization effect once the WC commits to the oxygen site. The value of

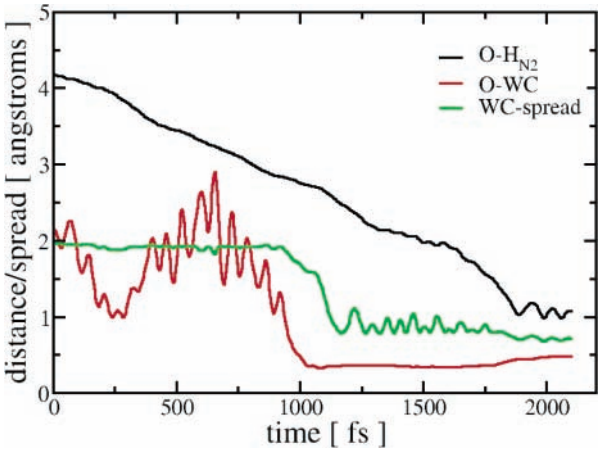

Figure 9. The evolution of the distances from the oxygen atom in the OH radical to the H_{N2} in guanine and the WC of the electron moving with H_{N2} during the hydrogen abstraction from the N2 in the condensed phase. Electron transfer is complete before the proton transfers. The spread of the WC is also shown; the electron was a π electron before transfer and localized around oxygen after transfer. Compared with Figure 8, the electron transfer is stabilized due to the surrounding water.

the WC spread is roughly equal to that found for the lone pairs within a solvated water environment, indicating nearly complete charge transfer.

We also attempted to examine the other possible reactions that could occur in the solvated environment. Because of the complexity of the solvated system, it is much more difficult to prepare the initial states and therefore only a limited number of starting points are sampled. In four attempts to study dehydrogenation in the presence of explicit waters, three trajectories spontaneously reacted within 3 ps. We also found, again, that all reactions including hydroxylation to the C8 site of guanine (see Figure 7) exhibited no barrier in our model of a solvated environment.

Thymine. We also performed calculations on the reactions of thymine with an OH radical using explicit waters. Because thymine is a smaller molecule, we draw from the solvated guanine calculations that an adequate model of solvation can be achieved starting with a well-equilibrated box of 32 waters for our purpose of studying radical reactions. Thus, the initial state of thymine was prepared in an identical fashion to the guanine, resulting in 25 solvating waters. In the gas phase, dehydrogenation from the C5 methyl site shows a concerted electron−proton loss (Figure 5). The transferred electron is a σ electron associated with a C−H bond and condenses to the oxygen atom as part of the O−H bond. The presence of the explicit water molecules does not alter the reaction mechanisms to a significant degree. Four trajectories are initiated from four randomly prepared different configurations. In one trajectory, the hydroxyl radical remains trapped in the solvent for the 6.5-ps simulation time, while the other three lead to successful dehydrogenation. To focus on the chemical reactions, we neglect from our analysis the trajectory that does not lead to reactions. In the three reacting trajectories, the hydroxyl radicals begin in different orientations with respect to the reacting C−H bond. Two of them lead to identical products via similar trajectories. The third one leads to an identical product but via a slightly different trajectory; the intermediate structure with the same C−H and H−O distances has a torsion angle (C−H−O−H) of −18° instead of 130° in the other two trajectories. The actual bond formation in the three reacting trajectories occur in the time scale of 20 fs; however, the diffusion time of the OH

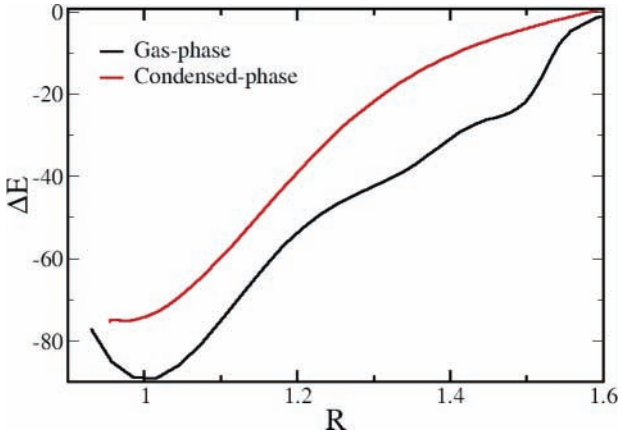

Figure 10. The change in the Kohn−Sham energy along the reacting coordinate for dehydrogenation at the C5 methyl group of thymine. Shown in the *x* axis is the distance from the oxygen atom in the OH radical to the H_{C5m} in thymine. The energy is in units of kJ/mol. Reactions in both the gas phase and the condensed phase (one successful trajectory is taken as representative) are shown, and there is no significant difference between the energy profiles.

radicals before bond formation occurs varies significantly from case to case and is at least 2 orders of magnitude slower.

Figure 10 plots the change in the Kohn−Sham energy along the reaction coordinate for dehydrogenation from the C5 methyl site in both the aqueous and gas phases. The similarities of these reactions path energies in the presence of polar solvent can probably be attributed to the fact that there are no charged intermediates present, which could be stabilized by solvents as in the case of dehydrogenation from guanine. This result is also consistent with our previous findings from the COSMO that inclusion of a polar solvent has a minimal effect on the reaction energetics for thymine hydroxylation. Thus, our prediction of a different gas-phase reaction mechanism for thymine as compared to guanine in the initial stages of damage via dehydrogenation seems also to hold in solvated conditions.

We also simulated the hydroxylation of thymine on the C5 site. Again, four trajectories are initiated from randomly prepared different configurations. Only one trajectory leads to hydroxylation, and the rest are trapped in the radical diffusion process for the 3-ps simulation time. In the successful trial, the reaction occurs without barrier and exhibits no significant differences from the gas phase. Although we do not have enough trajectories for a rigorous analysis of the reaction energetics, we predict hydroxylation on thymine to be less favorable than dehydrogenation from our dynamical simulations. This is consistent with our static quantum chemical studies with the COSMO method.

Conclusions

In this study, we performed a comparison of static and dynamical ab initio methods to determine the reaction mechanisms of DNA-base damage in the presence of an OH radical. We predict that the thermodynamically preferred site for dehydrogenation is the thymine C5 methyl and that the preferred sites for hydroxylation are at the C5 and C6. These predictions agree with available experimental data. We found that the relative energies of the thymine dehydrogenation and hydroxylation reaction products are sensitive to the choice of exchange and correlation functional or method of including electron correlation, especially for the higher-energy products. By use of power spectrum analysis, we verified that a model of solvated guanine in the presence of 21 waters was enough to adequately reproduce the first solvation shell, which may be important for the chemical reactions under study. Our results suggest different mechanisms of OH radical attack on thymine and guanine; thymine undergoes σ electron density loss for dehydrogenation, while guanine undergoes charge transfer, yielding a transient OH^- intermediate that subsequently abstracts a proton from the guanine cation. For the case of concerted proton−electron transfer found in thymine, no qualitative differences were found between the reaction mechanisms in the gas and solvated phases. For the separate proton−electron transfer in the mechanisms leading to guanine base damage, we found a propensity for complete charge transfer of a π electron to the OH radical in the solution phase simulations.

Acknowledgment. This work was performed under the auspices of the U.S. Department of Energy by Lawrence Livermore National Laboratory under Contract W-7405-ENG-48 and was funded by the Laboratory Directed Research and Development Program at Lawrence Livermore National Laboratory.

References and Notes

(1) *Advances in cell aging and gerontology*; Elsevier: New York, 2001; Vol. 4.
(2) Steenken, S.; Jovanovic, S. V. *J. Am. Chem. Soc.* 1997, *V119*, 617.
(3) Vialas, C.; Pratviel, G.; Claparols, C.; Meunier, B. *J. Am. Chem. Soc.* **1998**, *V120*, 11548.
(4) Yoshioka, Y.; Kitagawa, Y.; Takano, Y.; Yamaguchi, K.; Nakamura, T.; Saito, I. *J. Am. Chem. Soc.* **1999**, *V121*, 8712.
(5) Cadet, J.; Delatour, T.; Douki, T.; Gasparutto, D.; Pouget, J. P.; Ravanat, J. L.; Sauvaigo, S. *Mutat. Res.* **1999**, *V424*, 9.
(6) Bamatraf, M. M. M.; O'Neill, P.; Rao, B. S. M. *J. Phys. Chem. B* **2000**, *V104*, 636.
(7) Candeias, L. P.; Steenken, S. *Chem.−Eur. J.* **2000**, *V6*, 475.
(8) Kuzmin, V. A.; Dourandin, A.; Shafirovich, V.; Geacintov, N. E. *Phys. Chem. Chem. Phys.* **2000**, *V2*, 1531.
(9) Chworos, A.; Coppel, Y.; Dubey, I.; Pratviel, G.; Meunier, B. *J. Am. Chem. Soc.* **2001**, *V123*, 5867.
(10) Weatherly, S. C.; Yang, I. V.; Thorp, H. H. *J. Am. Chem. Soc.* **2001**, *V123*, 1236.
(11) Wagner, J. R.; Vanlier, J. E.; Berger, M.; Cadet, J. *J. Am. Chem. Soc.* **1994**, *116*, 2235.
(12) Douki, T.; Spinelli, S.; Ravanat, J. L.; Cadet, J. *J. Chem. Soc., Perkin Trans.* **1999**, *2*, 1875.
(13) Close, D. M.; Eriksson, L. A.; Hole, E. O.; Sagstuen, E.; Nelson, W. H. *J. Phys. Chem. B* **2000**, *V104*, 9343.
(14) Wetmore, S. D.; Boyd, R. J.; Eriksson, L. A. *J. Phys. Chem. B* **1998**, *V102*, 9332.
(15) Wetmore, S. D.; Boyd, R. J.; Eriksson, L. A. *J. Phys. Chem. B* **1998**, *V102*, 5369.
(16) Wetmore, S. D.; Himo, F.; Boyd, R. J.; Eriksson, L. A. *J. Phys. Chem. B* **1998**, *V102*, 7484.
(17) Wetmore, S. D.; Boyd, R. J.; Himo, F.; Eriksson, L. A. *J. Phys. Chem. B* **1999**, *V103*, 3051.
(18) Wetmore, S. D.; Boyd, R. J.; Eriksson, L. A. *Chem. Phys. Lett.* **2000**, *322*, 129.
(19) Prat, F.; Houk, K. N.; Foote, C. S. *J. Am. Chem. Soc.* **1998**, *V120*, 845.
(20) Becke, A. D. *J. Chem. Phys.* **1993**, *98*, 5648.
(21) Mundy, C. J.; Colvin, M. E.; Quong, A. A. *J. Phys. Chem. A* **2002**, *V106*, 10063.
(22) Car, R.; Parrinello, M. *Phys. Rev. Lett.* **1985**, *55*, 2471.
(23) Hutter, J.; Ballone, P.; Bernasconi, M.; Focher, P.; Fois, E.; Goedecker, S.; Parrinello, M.; Tuckerman, M. E. *CPMD code, version 3.3*; MPI fuer Festkoerperforschung: Stuttgart and IBM Zurich Research Laboratory, 1990−1996.
(24) Pasquarello, A.; Laasonen, K.; Car, R.; Lee, C. Y.; Vanderbilt, D. *Phys. Rev. Lett.* **1992**, *69*, 1982.
(25) Laasonen, K.; Pasquarello, A.; Car, R.; Lee, C.; Vanderblit, D. *Phys. Rev. B* **1993**, *47*, 10142.
(26) Hartwigsen, C.; Goedecker, S.; Hutter, J. *Phys. Rev. B: Condens. Matter* **1998**, *V58*, 3641.
(27) Sprik, M.; Hutter, J.; Parrinello, M. *J. Chem. Phys.* **1996**, *V105*, 1142.
(28) Becke, A. D. *Phys. Rev. A: Gen. Phys.* **1988**, *38*, 3098.
(29) Lee, C.; Yang, W.; Parr, R. G. *Phys. Rev. B: Condens. Matter* **1988**, *37*, 785.

(30) Berghold, G.; Mundy, C. J.; Romero, A. H.; Hutter, J.; Parrinello, M. *Phys. Rev. B* **2000**, *V61*, 10040.
(31) Perdew, J. P.; Burke, K.; Ernzerhof, M. *Phys. Rev. Lett.* **1996**, *77*, 3865.
(32) Troullier, N.; Martins, J. L. *Phys. Rev. B* **1991**, *43*, 1993.
(33) Vanderbilt, D. *Phys. Rev. B* **1990**, *41*, 7892.
(34) Tassone, F.; Mauri, F.; Car, R. *Phys. Rev. B: Condens. Matter* **1994**, *50*, 10561.
(35) Wu, Y. PhD Dissertation, Department of Chemistry, Princeton University, 2004.
(36) Barone, V.; Cossi, M. *J. Phys. Chem. A* **1998**, *102*, 1995.
(37) Frisch, M. J.; Trucks, G. W.; Schlegel, H. B.; Scuseria, G. E.; Robb, M. A.; Cheeseman, J. R.; Zakrzewski, V. G.; Montgomery, J. A., Jr.; Stratmann, R. E.; Burant, J. C.; Dapprich, S.; Millam, J. M.; Daniels, A. D.; Kudin, K. N.; Strain, M. C.; Farkas, O.; Tomasi, J.; Barone, V.; Cossi, M.; Cammi, R.; Mennucci, B.; Pomelli, C.; Adamo, C.; Clifford, S.; Ochterski, J.; Petersson, G. A.; Ayala, P. Y.; Cui, Q.; Morokuma, K.; Malick, D. K.; Rabuck, A. D.; Raghavachari, K.; Foresman, J. B.; Cioslowski, J.; Ortiz, J. V.; Stefanov, B. B.; Liu, G.; Liashenko, A.; Piskorz, P.; Komaromi, I.; Gomperts, R.; Martin, R. L.; Fox, D. J.; Keith, T.; Al-Laham, M. A.; Peng, C. Y.; Nanayakkara, A.; Gonzalez, C.; Challacombe, M.; Gill, P. M. W.; Johnson, B. G.; Chen, W.; Wong, M. W.; Andres, J. L.; Head-Gordon, M.; Replogle, E. S.; Pople, J. A. *Gaussian 98*, revision A.4; Gaussian, Inc.: Pittsburgh, PA, 1998.
(38) Baik, M. H.; Silverman, J. S.; Yang, I. V.; Ropp, P. A.; Szalai, V. A.; Yang, W. T.; Thorp, H. H. *J. Phys. Chem. B* **2001**, *V105*, 6437.
(39) Kasende, O. E.; Szczepaniak, S.; Person, W. B.; Zeegers-Huyskens, T. *J. Mol. Struct.* **1997**, *435*, 17.
(40) Gaigeot, M.-P.; Sprik, M. *J. Phys. Chem. B* **2003**, *107*, 10344.
(41) Silvestrelli, P. L.; Parrinello, M. *Phys. Rev. Lett.* **1999**, *V82*, 5415.